



Received: 21 March 2018  
Accepted: 23 October 2018  
First Published: 31 October 2018

\*Corresponding author: Timothée Miyouna, Marien NGOUABI University, PO Box 69, Brazzaville, Republic of Congo E-mail: [miyounatim@yahoo.fr](mailto:miyounatim@yahoo.fr)

Reviewing editor:  
Robin John Armit, School of Earth,  
Atmosphere and Environment,  
Monash University, Australia

Additional information is available at  
the end of the article

## SOLID EARTH SCIENCES | RESEARCH ARTICLE

# Strike-slip deformation in the Inkisi Formation, Brazzaville, Republic of Congo

Timothée Miyouna<sup>1\*</sup>, Hardy Medry Dieu-Veill Nkodia<sup>1</sup>, Olivier Florent Essouli<sup>1</sup>, Moussa Dabo<sup>2</sup>, Florent Boudzoumou<sup>1,3</sup> and Damien Delvaux<sup>4</sup>

**Abstract:** Evidence of strike-slip deformation in the Inkisi Formation was overlooked for a long time. After controversial characterization, this paper demonstrates that the Inkisi Formation underwent at least two phases of strike-slip deformation accompanied with a compressive component, which created faults that help determine paleostress. Field observations permitted to characterize NW–SE trends sinistral strike-slip faults systems and NE–SW oriented dextral strike-slip faults systems. The strike-slip faults are associated with flower structures in profile view and with damage zones along tips, wall and linking zones in plan view. Both faults systems (sinistral and dextral) initiated from joints, which show similar orientations with faults. Many kinematic indicators of slip sense or extension have enabled to determine the stress stages and the evolution of the structures. The first tectonic phase has a horizontal maximum principal compressive stress  $\sigma_1$  of  $319 \pm 21,1/03$ , which probably have a potential correlation with far-field stress propagation which occurs during the subduction of Gondwana south margin in the Permo-Trias. The second tectonic phase with a slightly inclined maximum principal compressive stress  $\sigma_1$  of  $264^\circ \pm 22,3/12$  potentially results from the intraplate stress propagation, due to the opening of the Southern Atlantic Ocean.

**Subjects:** Earth Sciences; Geology – Earth Sciences; Sedimentology & Stratigraphy

**Keywords:** strike-slip faults; joints; damage zones; plumose structures; flower structure; paleostress; Inkisi formation; Congo

### 1. Introduction

Characterization of strike-slip deformation has increased worldwide, as their fault zone characteristics has been proven to have a significant control on fluid flow and earthquakes initiation and termination. These studies evolved with proposition of several examples and models of fault growth and propagation (Kim et al., 2000; Martel, 1990; Olson & Pollard, 1991; Pollard & Aydin, 1988; Segall & Pollard, 1983). These models include characterization of different types of

### ABOUT THE AUTHOR

Timothée Miyouna is an assistant professor at Marien NGOUABI University of Brazzaville, where he teaches mineralogy and petrology of sedimentary rocks. He extensively worked in gold mineralization in West Africa Belt. Actually, he is working in basin researches and tectonic deformations in the Paleozoic sandstones of Inkisi.

### PUBLIC INTEREST STATEMENT

The study of the tectonic structures that affected the Inkisi sandstone of Paleozoic age, in the southern Brazzaville has a paramount importance. A large part of the city is built on these sandstones that carry fractures that reach the topographic surface. This constitutes a large danger to the buildings and the stability of the geotechnical structures. This study can also be a good guideline in groundwater exploration.

structures that occur (Christie-Blick & Biddle, 1985; Kim, Peacock, & Sanderson, 2004; Slyverster, 1988) both in plan view and in cross-section around strike-slip faults. Particularly, identification of damage zones structures around strike-slip faults has been subject to classification by Kim and al. (2004). This classification, proven to be reliable, has been applied to the less studied Inkisi Formation in Republic of Congo in order to identify sets of fractures that affect this Formation.

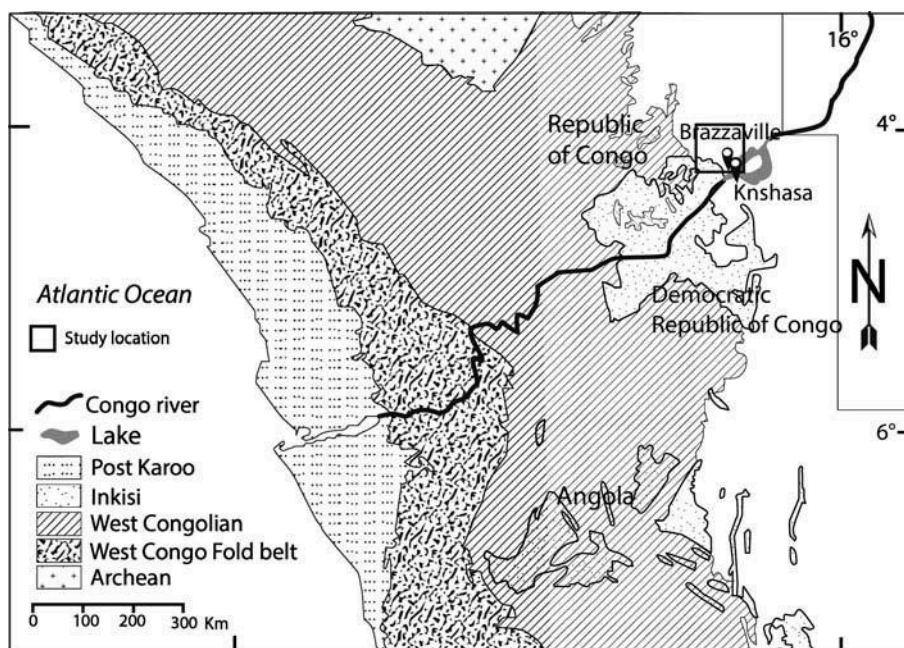
Previous studies on the Inkisi Formation have first revealed two sets of orthogonal non-described fractures (Dadet, 1969). Then these fractures were subject of two controversial considerations according to their characterization. They were first considered as faults by Cornet and Pourret (1982) without specifying their classification types, and then reconsidered as syndimentary hydroplastic faults by Alvarez, Maurin, and Vicat (1995). The latter characterization implies that the Inkisi Formation has not undergone a tectonic event. Nonetheless, in Angola, the Inkisi Formation is overlain by Karoo deposits Formation of Permian age (Oesterlen, 1976), which are widespread in the southern Sahara Desert of Africa (Tack et al., 2001), but Karoo deposits are deformed in most part of Africa in the Congo basin and in rift segments of Tanganyika–Rukwa–Malawi (Catuneanu et al., 2005; Catuneanu, 2004; Daly, Lawrence, Dirmu-Tshiband, & Matouana, 1992; Daly, Lawrence, Kimun'a, & Binga, 1991; Delvaux, 2001a, 2001b; Delvaux, Kervyn, Macheyeke, & Temu, 2012). Thus, it necessarily implies that the underlying unit of Inkisi Formation would be deformed also.

This paper firstly presents a characterization of joints and strike-slip faults by description of different types of damage zones around faults according to the classification of Kim et al. (2004) and their profile view description. Secondly, we present the different fracture systems and determine paleostress with the Win-Tensor program, using the stress inversion method (Delvaux, 1993). At the end, we prove that strike-slip faults nucleate from joints.

## 2. Geological sitting

The Inkisi Formation extends from Republic of Congo to Angola via Democratic Republic of Congo (Figure 1). It outcrops in the southern part of Brazzaville along the Congo river. It overlays the Congo craton, which is of Archean age, where it is separated by an angular unconformity with underlying units of West Congolian Group, a foreland part of the Panafrican West Congo Orogen (from 625Ma to 490Ma) (Dadet, 1969; Alkmim et al., 2006).

**Figure 1. Location of the studied area (black square) and the distribution of the Inkisi Formation over the Central Africa. Redrawn after Dadet (1969).**



The Inkisi Formation is also part of the “redbeds” sequence in the Congo basin of 1000 m of thickness, where it is correlated with Banalia Group in the Lindi Basin in RDC (Figure 2) and the Banio group in Central Africa Republic (Delpomdor & Pr at 2015; Kadima et al., 2011; Tack et al., 2008). These three correlated units show arkoses of same types of sedimentary structures.

The Inkisi Formation is considered as an individual lithological unit unrelated to Pan-African orogeny (Tack, Wingate, Li geois, Fernandez-Alonso, & Deblond, 2001). The age of the Inkisi Formation is not well constrained. However, it is suggested of pre-Karoo age (320Ma) (Tack et al., 2008), because in Angola the Inkisi Formation is overlain by Karoo deposits of Permian age (Oesterlen, 1979). Affaton et al. (2016) in Congo Brazzaville suggested a deposition U-Pb age, obtained through detrital zircon between 500 and 800 Ma. However, in Democratic Republic of Congo, Frimmel et al. (2006) suggested U-Pb ages between 558 and 851 Ma. Therefore, the Inkisi Formation seems to be of earlier Paleozoic age.

**Figure 2. Lithostratigraphic synthesis of Neoproterozoic to Early Paleozoic period of geological units that overlies the Congo Craton, in Republic of Congo. Compiled after Dadet (1969), Dianzenza-Ndefi (1983), Boudzoumou, (1986), Frimmel et al. (2006), Poidevin (2007), Straathof (2011), Tait et al. (2011), Mickala et al. (2014).**

Age (MA)	Units of West Congo regions			
	SuperGroup	Group	Lithology	
~320			<b>Karoo deposits</b>	
558 to 851 (Frimmel et al., 2006)	Early Paleozoic	Inkisi	Sandstones, intercalated conglomerates.	
			Tectonic uncoformity (Pan-African orogeny ~635MA)	
566±46 (Straathof, 2011)	Late Neoproterozoic	West-Congo SuperGroup	Mpioka	Shales, siltstones, sandstones conglomerate at base.
575 (Poidevin, 2007)			Schlusto-Calcaire	Limestones, dolomites, oolites, cherts, and intercalations of shales and marns
635 (Mickala et al., 2014)	Late Neoproterozoic		Upper Diamictite	Glacial diamictite
1113 to 901 (Dianzenza-Ndefi, 1983)			Bouenzian	Cross-Bedded sandstones, clays, and conglomerates
			Lower Diamictite	Glacial diamictite
910 to 1000 (Tait et al., 2011)	Proterozoic			West Congo Orogen
2500 (Dianzenza-Ndefi, 1983)	Archean			Congo Craton

Alvarez et al. (1995) after a thorough facies description concluded that the Inkisi Formation corresponds to a large deltaic body, but these assertions still debatable as the pro-delta is currently missing in the sequence. However, a well-defined subdivision of Inkisi Formation which agrees with our field observations was done by Boudzoumou (1986). He suggested that the Inkisi Formation is of fluvial origin, and it is made up of repeatedly three terms: (i) coarse sandstones associated with quartzite elliptical pebbles, which sometimes show in its lower part conglomerates; (ii) coarse sandstone with trough cross-bedding; and (iii) alternating fine sandstones to very fine sandstone with horizontal laminations.

The studied area is located in south west of Brazzaville, in the Republic of Congo (Figure 1). Fractures have been recorded in the artisanal quarries of Brossete and Kombé along the Congo river.

### 3. Methodology

The methodology was developed from literature on features of joints and strike-slip faults. The collection of data were done on the field. Then data analyses were computed in programs.

#### 3.1. Field data collection

The collection proceeds first by searching of geological structures. Once found, geographic coordinate of the station was taken. Then we identified faults and joints: firstly by a geometric analysis, by recording their orientation, their architecture, their connections and secondly by a kinematic analysis by looking offsets features (pebbles, etc.), secondary structures along the traces of structures and by looking for slip sense of slip indicators on the surfaces of faults. After a characterization, a sketch of these structures was produced and recorded measurements of structures (by Topochaix compass) were put in the sketch. At the end, photographs of field evidence on identified structures were taken and their number reported on the sketch.

#### 3.2. Data analysis

Data were first recorded in a summary table of measurements with Excel program. Then we produced histograms from strikes measurements. The Win-Tensor program, version: 5.8.8 was used to produce rose diagrams, stereograms and to determine paleostress (Delvaux, 1993). The determination of paleostress from the Win-Tensor program used the stress inversion method (Angelier, 1994, 1989) which complies with the procedure described in Delvaux and Sperner (2003). The stress inversion method helps reconstitute four parameters of the reduced tensors:  $\sigma_1$ ;  $\sigma_2$ ;  $\sigma_3$  (where  $\sigma_1 \geq \sigma_2 \geq \sigma_3$ ) and the ratio  $R = (\sigma_2 - \sigma_3)/(\sigma_1 - \sigma_3)$  (where  $0 < R < 1$ ), which determine the intensity of  $\sigma_2$  relative to  $\sigma_1$ ; and  $\sigma_3$ . The program determines the index regime called  $R'$  based on the ratio  $R$  and on a vertical continuous scale from 0 (radial extension) to 3 (constriction), with  $R' = R$ , for an extension regime (0 to 1);  $R' = 2 - R$  for a strike-slip regime (1 to 2);  $R' = 2 + R$  for a thrust regime (2 to 3). The reduced tensor is first estimated by Right dihedral method. They are more precisely determined with an iterative rotational stress optimization. The program assesses the quality of the obtained tensors from two qualities ranking parameter QR. The first, the QRw, which is a quality rank defined as in World Stress Map project, it ranges from A (best); B (good), C (medium), D (poor) to E (worst). It is determined in function of threshold values of series of criteria (Delvaux et Sperner, 2003). The second, the QRt, is a quality rank of diversity of faults orientation and the found slip lineation. The program uses several criteria to evaluate the ranking quality, as well described in Delvaux et Sperner (2003).

Data were input manually in the program, as characterized in the field, as fault with slip line, shear plane with tension failure, shear fractures and joints (see Table A1). Additionally, we carry out a grouping into primary subsets, according to field criteria (cross-cutting principle, relative age, reactivation, neof ormation, etc.). Furthermore, after processing, the program suggests an optional data separation into secondary subsets of homogeneous orientation of initially chosen subsets.



## 4. Field data results and faults patterns

### 4.1. Strike-slip faults

Strike-slip faults form two major sets of fractures that cross cut each other at varying angle (from acute to almost orthogonal). The first set is made up of sinistral strike-slip faults and has strike orientation that ranges from 335° to 019° (Figure 3b, c). The second set is made up of dextral strike-slip faults and has strike orientation ranging from 020° to 065° (Figure 4b, c). Both sets show a steep dip, ranging from 70° to 90° and their major line plunge at to 5° (Figure 3a, d; 4a, d). The polished surfaces of faults are generally filled with palygorskite and calcite (Figure 5c), accretion steps of calcites (Figure 5a) and show within some surfaces crystal fiber lineation (Figure 5b).

**Figure 3. Rose diagrams and stereograms of sinistral strike-slip faults. Three classes of orientations Z1a, Z1b, and Z1c were distinguished.**

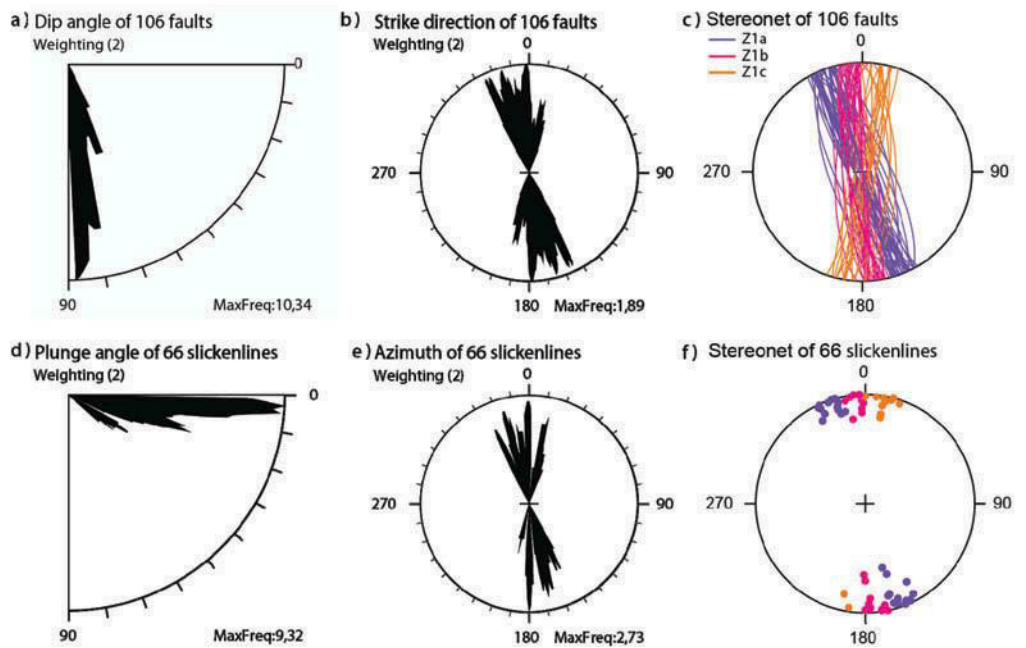
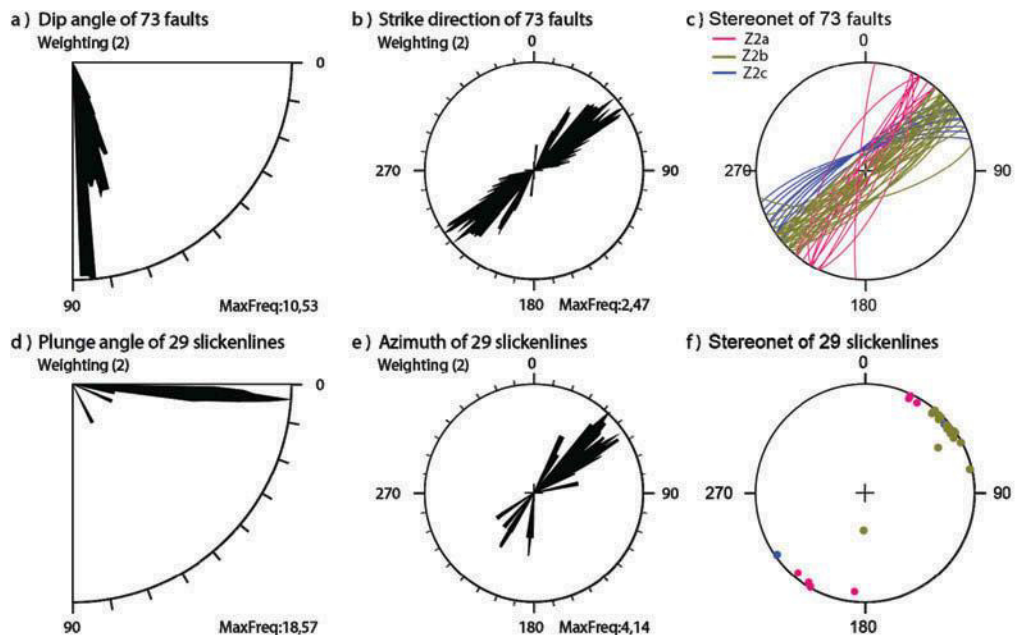


**Figure 4. Rose diagrams and stereograms of dextral strike-slip faults. Three classes of orientations Z2a, Z2b, and Z2c were distinguished.**



Through their traces, they showed many kinematic indicators that help inferred the sense of movement, as displaced pebbles (Figure 6), pull-apart structures, horstailing splays, etc.

Both strike-slip faults show a progression from single small faults with little displacement (7 mm) to faults zones of moderate displacement (up to 12 cm) and length (up to 400 m). In horizontal plan view, both sets of strike-slip faults (dextral and sinistral) show subparallel faults which relayed each other, associated with bends and characteristic feature of fault damage zones around their tips, linking zones and wedge zones. In cross-section view, both sets show negative and positive flower structures; however, sinistral strike-slip faults showed frequently positive flower structures, while dextral strike-slip faults showed negative structures flowers numerously. Fault damage structures are well expressed by sinistral strike-slip faults, which form compound strike-slip fault zones (Figure 7), as described by Martel (1990). Compound strike-slip faults are presumed to accommodate larger displacement than other faults (Martel, 1990). Figure 8 shows the relationship of two set fractures. The sinistral strike-slip faults are

**Figure 5. Strike-slip fault surfaces and kinematic indicators. (A) Slickensides highlighted by accretion steps of calcite, or (B) crystal fiber stretching. (C) A left-step sinistral strike-slip with palygorskite and overprint slickensides in its surface show details in (D).**



**Figure 6. Displaced pebbles within strike-slip faults. (A) Sinistral lateral strike-slip faults with 2 cm of displacement. (B) Dextral strike-slip faults with a small vertical component.**

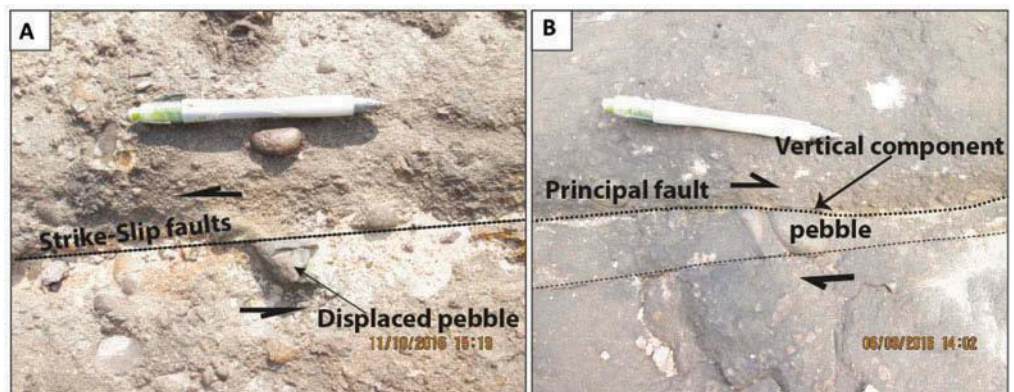
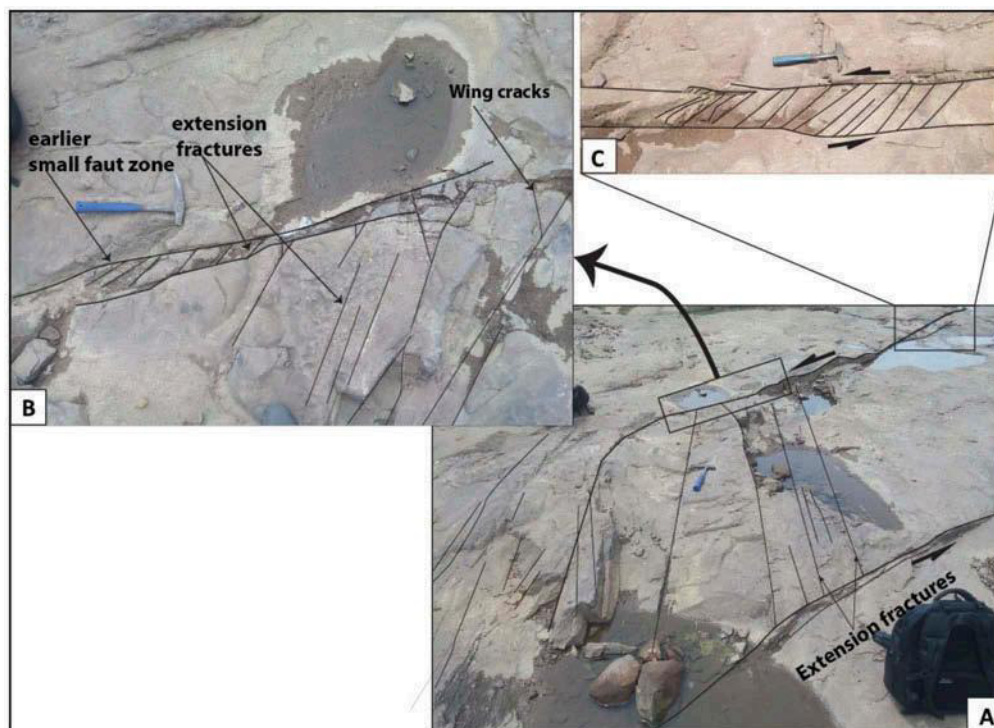


**Figure 7. Compound fault zone associated with small fault zone. (A) Compound fault zone with extension fractures. (B) Small fault zone within boundaries of compound fault zone and extension fractures showing wing crack terminations that overprint small fault zone. (C) Another small fault zone with extensions fractures at the tip of the compound fault zone.**



crossed-cut and displaced by the dextral strike-slip faults. More than five zones of this type were found with a displacement ranging between 2cm and 5cm.

#### 4.1.1. Tip zones damage structures

4.1.1.1. *Horsetail splays and en-echelon fractures.* Faults display in some places horsetail fractures at their tips (Figure 9). The angles between the main faults and the horsetail fractures range from 20° to 45°. The local orientation of the maximum compressive stress has been assumed to be parallel to horsetail fractures (320° for sinistral fault). Some horsetail fractures show a normal slip component within their traces, a change in their orientation, and wing cracks development at their intersection with the main fault. Wing cracks development within horsetail fractures tips imply that they formed from mode I loading.

En-echelon fractures (Figure 9) can be associated with extensions fractures. They are assumed to propagate away from the fault terminations and they show steep dip.

#### 4.1.2. Linking damage zones

They are dominated by extension fractures, dilation jogs and pull-apart structures.

4.1.2.1. *Extension fractures.* They dominantly link faults (Figure 10) and are assumed to develop parallel to the maximum compressive stress  $\sigma_1$ . The angles between main faults and extensions fractures range from 40 to 55°. Some of them of wing crack at their intersection with the principal fault. A principal fault might be associated both with extensions fractures and horsetail fractures. The identification of extensions fractures is supported by the presence of wing cracks at the intersection with main fault and additionally, by range of their intersection angle (40° to 55°) with main faults, as described by Hancock (1985). They constitute the type of structures most frequently observed in the field and help greatly to determine paleostress.



**Figure 8.** Cross-cutting relationship between sinistral strike-slip fault and dextral strike-slip fault. The sinistral strike-slip fault is displaced by dextral strike-slip over 2 cm of offset. (A) Cross-cutting relationship. (B) Sketch of cross-cutting relationship of sinistral fault (Z1) and dextral fault (Z2) in A. (C) and (D) Corrugation (b) and crushed rock (a) within the surface of Z2.

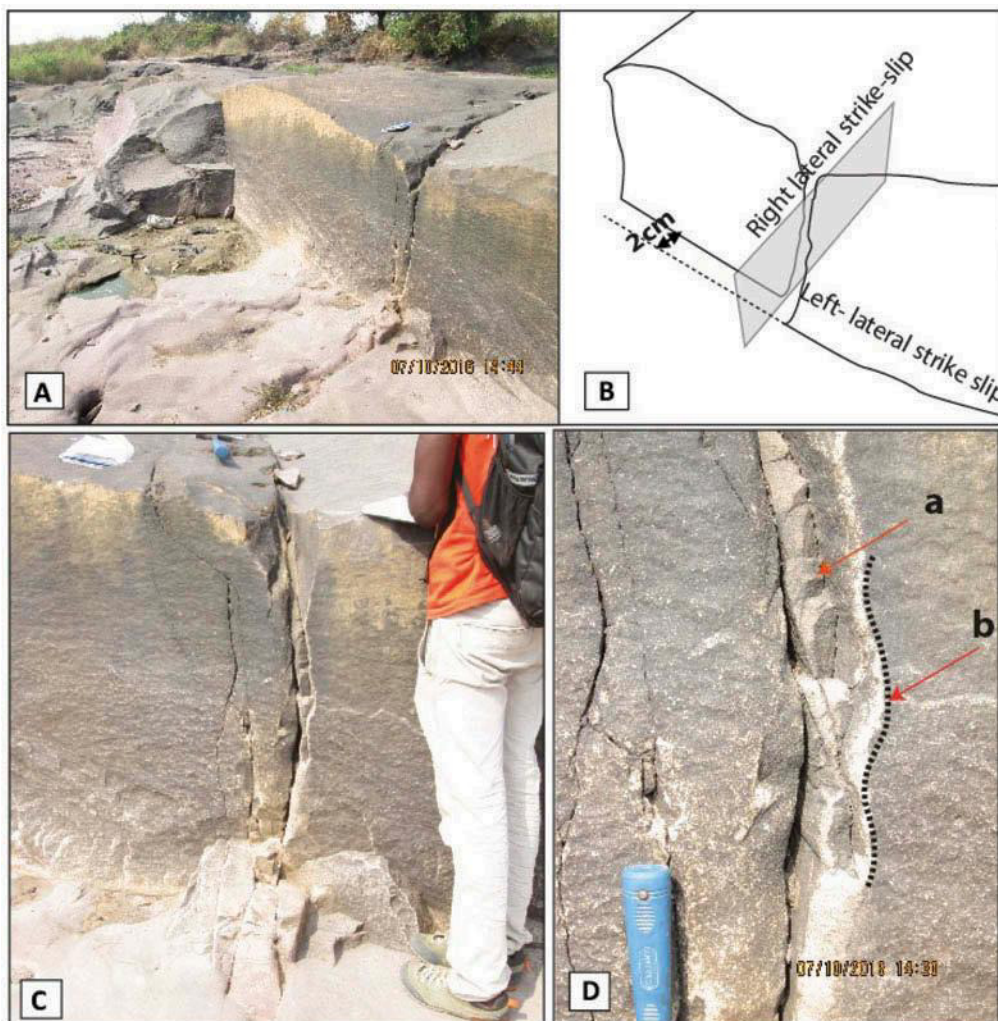


**Figure 9.** (A): Horsetail splays at 190/85 oriented dextral strike-slip fault tip. (B) En-echelon fractures at sinistral strike-slip fault tip.

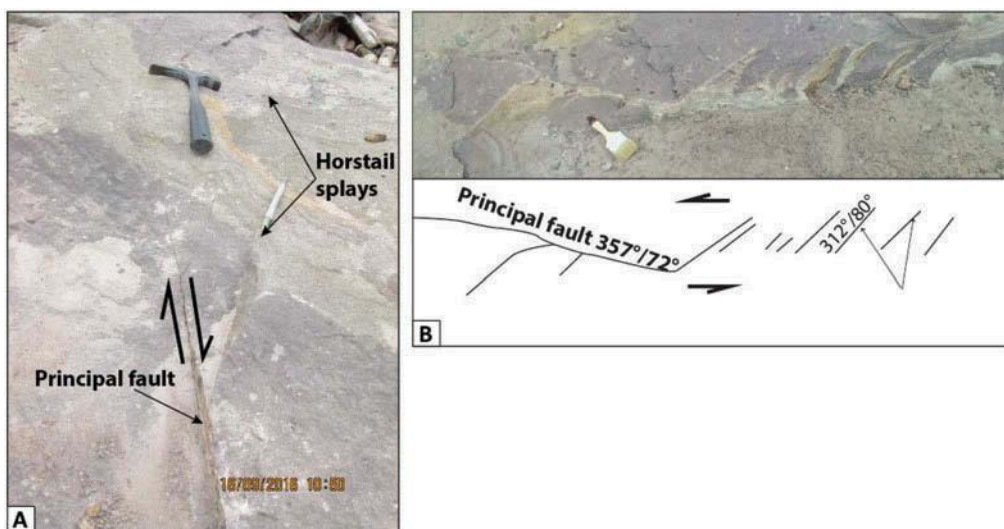
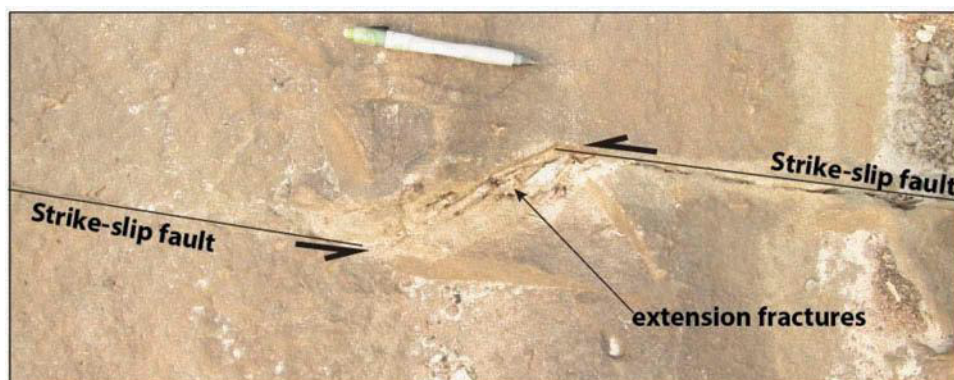




**Figure 10.** Extension fractures around linking zone of a sinistral strike-slip fault, observed in horizontal plan view.



4.1.2.2. *Dilation jogs.* They appear most of time within the fault traces (Figure 11). They often show lens shape with crushed material and duplex.

4.1.2.3. *Pull-apart.* Pull-apart structures (Figure 12) are extension fractures that opened up between two linked faults due to increasing slip in fault segment (Kim et al., 2004). They show a normal component in their interior, suggesting an opening. The geometric shape is controlled by boundary fractures.

#### 4.1.3. *Wall damage zone*

Wall damage zone as linking damage has sometimes quite similar architecture. We find extension fractures intersecting two faults traces as in linking damage zone, but here no relay zones, only two bounding strike-slip faults. Extension fractures show also wing crack at their intersection with the main fault (Figure 13).

**Figure 11.** Dilation jog around strike-slip fault.



**Figure 12.** Pull-apart structure associated with a dextral strike-slip fault.

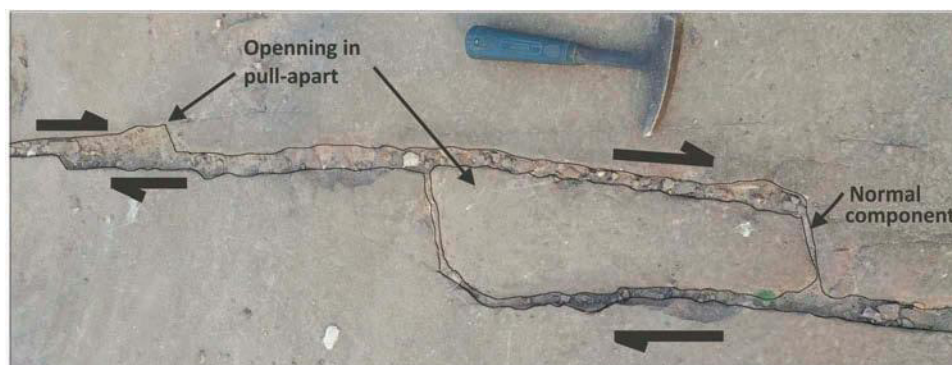


**Figure 13.** Strike-slip fault showing both a wall damage zone with extension fractures and horsetail splay fractures at its tips. Note wing cracks on extension fractures.



#### 4.1.4. Flower structures

They have been first noticed as lens shaped in plan view, and then observed in profile view at least two or three plans of fractures that bifurcate from one steep fault. Bifurcated planes delimit a space which frequently comprises lots of fractures. Most of the fractures within the space show characteristics of negative flower structures (Figure 14) with normal-slip component. Flower structures have same orientation relation to strikes of both strike-slip faults systems.

#### 4.2. Joints

Joints show parallel orientation with strike-slip faults (Figure 15b, c). They are predominantly steeply dipping (Figure 15a). Therefore, they were subdivided into two sets: one parallel to sinistral strike-slip faults (Figure 15d, e) and the other parallel to dextral strike-slip (Figure 15f). Figures 15 and 16 show rose diagrams and stereograms that support this evidence. At least 16% of joints were found with well-marked plumose structures (Figures 17, 18). Most plumose structures display straight plume axis, and seemed to originate from pebbles or micro-cracks in the rock. Some plumose structures show fine hackles to more noticeable ones within the joint planes. Apart from straight plumes, plumes with many arrest lines have been found (Figure 18a). Some plumose structures have been found with slickensides overprinting them (Figure. 18b, c) as it was described

**Figure 14. Flower structures associated with a dextral strike-slip faults.**



**Figure 15. Rose diagrams and stereograms of joints without plumose structures (a,b,c). Distinction of five subsets (a,b,c,d,e,f).**

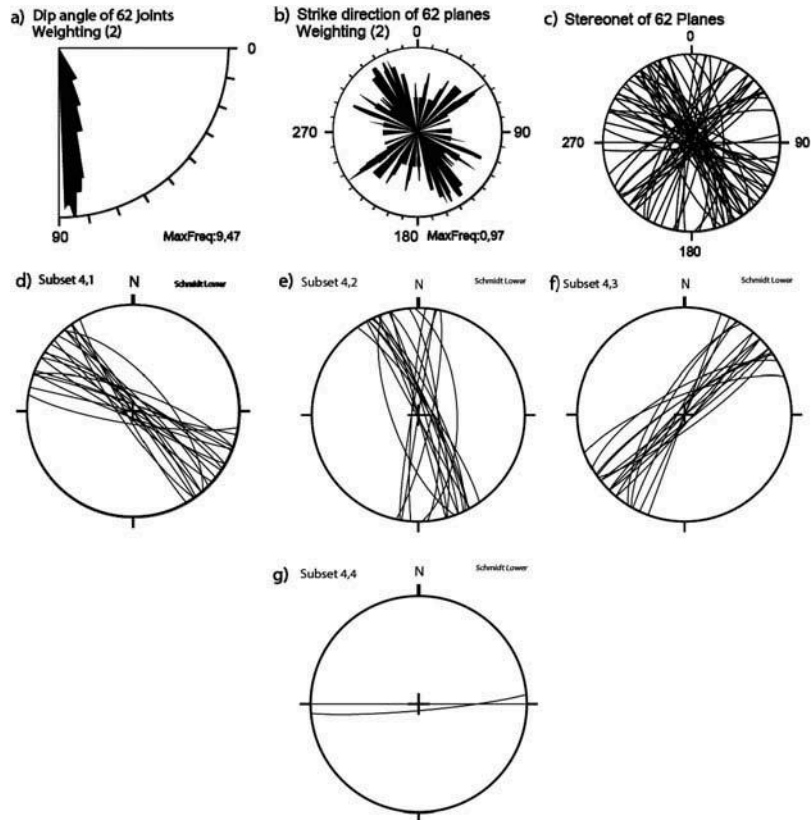




**Figure 16. Rose diagrams and stereograms of joints with plumes structures (a,b,c). Distinction of different subsets (d,e,f).**

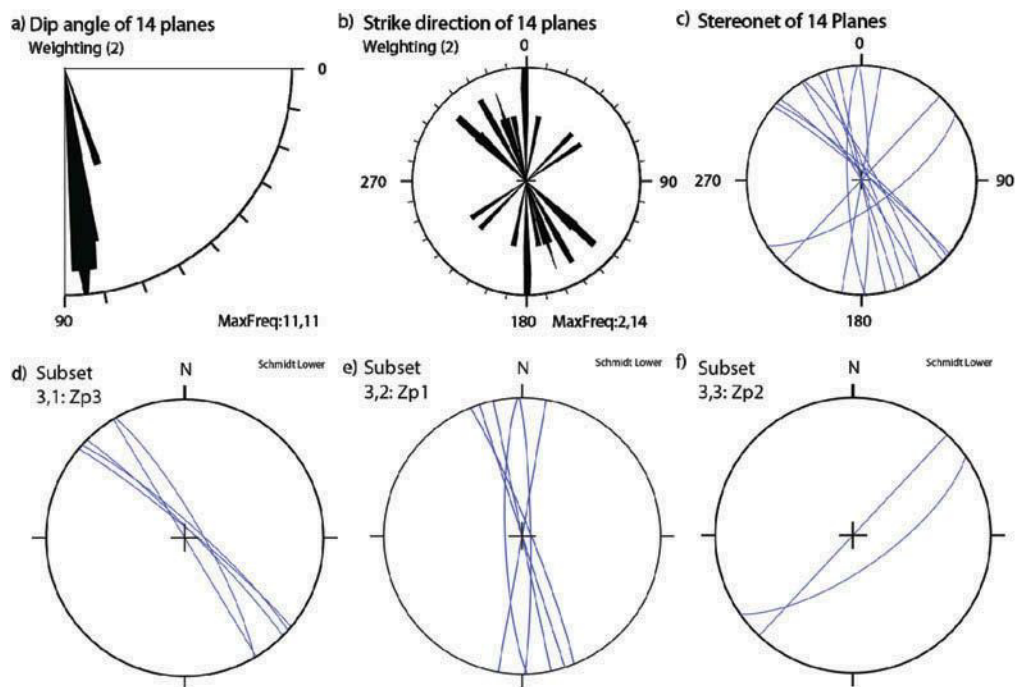
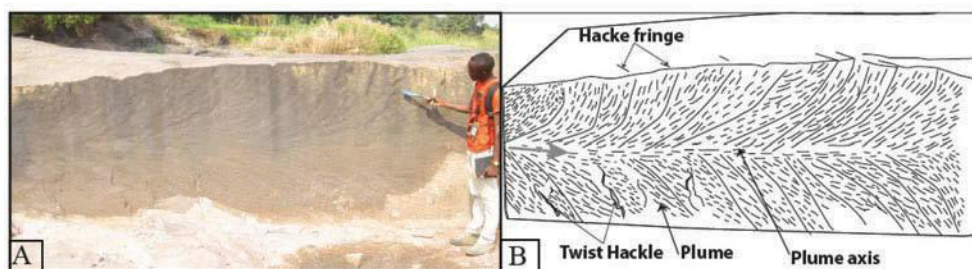


**Figure 17. Plumose structures with weakly marked hackle. (B) Sketch of the photo, with the grey arrow showing the propagation direction.**



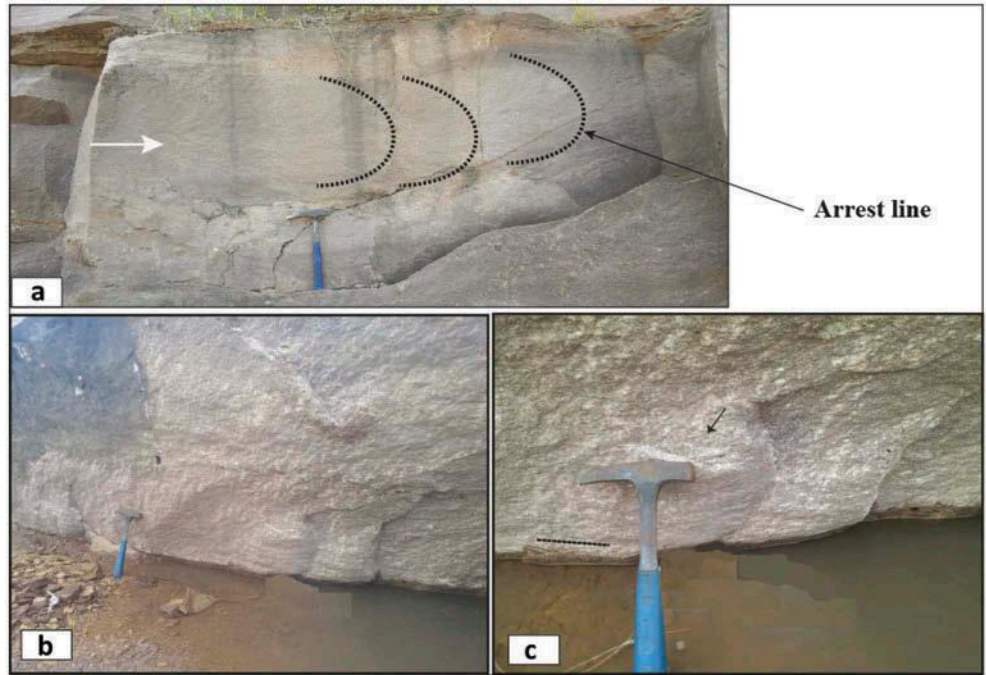
by Barton (1983) and Segall and Pollard (1983). This evidence indicates at least two fault phases of deformation (Pollard & Aydin, 1988). Plumose joints with many arrest lines have also through their surface decimetric veins of calcite.

### 5. Results of stress inversion

Measurements were grouped into four (04) subsets: (1) subset of sinistral strike-slip (Z1); (2) subset of dextral strike-slip (Z2); (3) subset of parallel joints to Z1; and (4) subset of parallel joints to Z2. From the four subsets, four stages of stress have been found. Chronologically these stages have to be grouped into two tectonic stress stages, because field observations suggested the evolution of joints into faults:

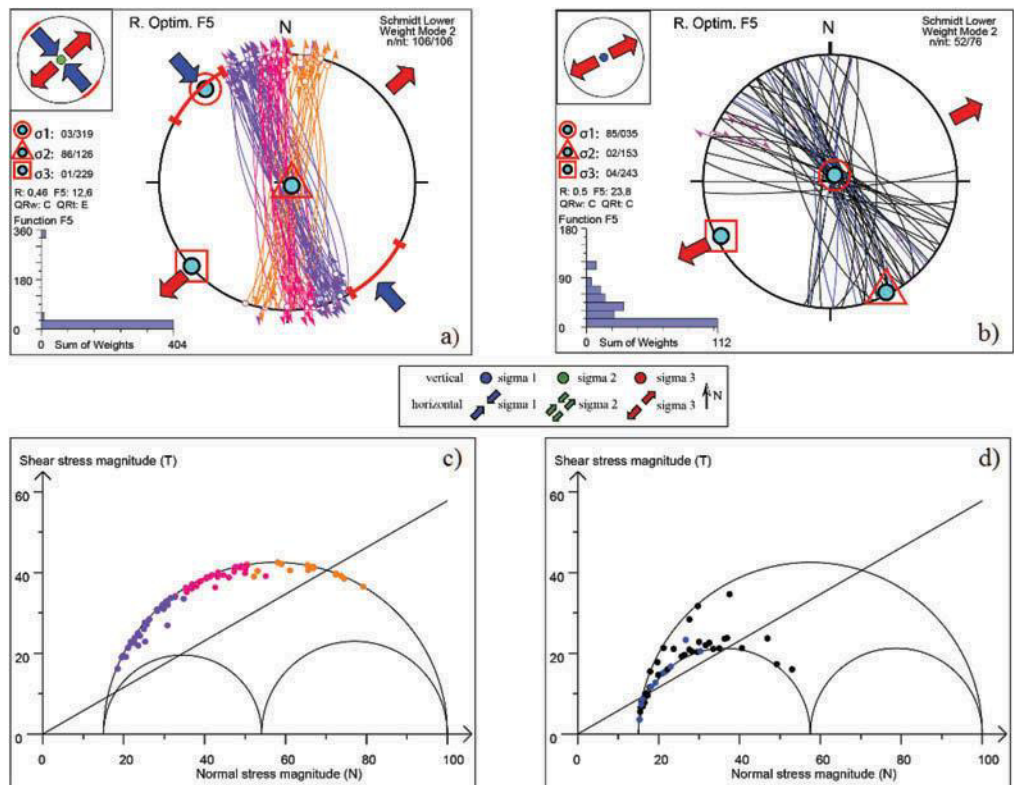
- Stress stage 1 (Figure 19): This is the oldest, represented by 182 fractures (106 faults and 76 joints), with 66 striated planes of faults. It started with an extension regime ( $R' = 0,5$ ) (Figure 19b) with NE-SW principal direction of extension, forming the majority of joints with plumes, the quality rank QRw and QRT of this stage are medium. The change in orientation of joints is probably due to rock defaults (Davis, Reynolds & Kluth, 2011). The passage from extension regime to strike-slip regime (Figure 19a) was achieved through a rotation of the maximum

Figure 18. (a) Plumose structures with many arrest lines. (b and c) Well-marked twist hackles with overprinted slickensides.

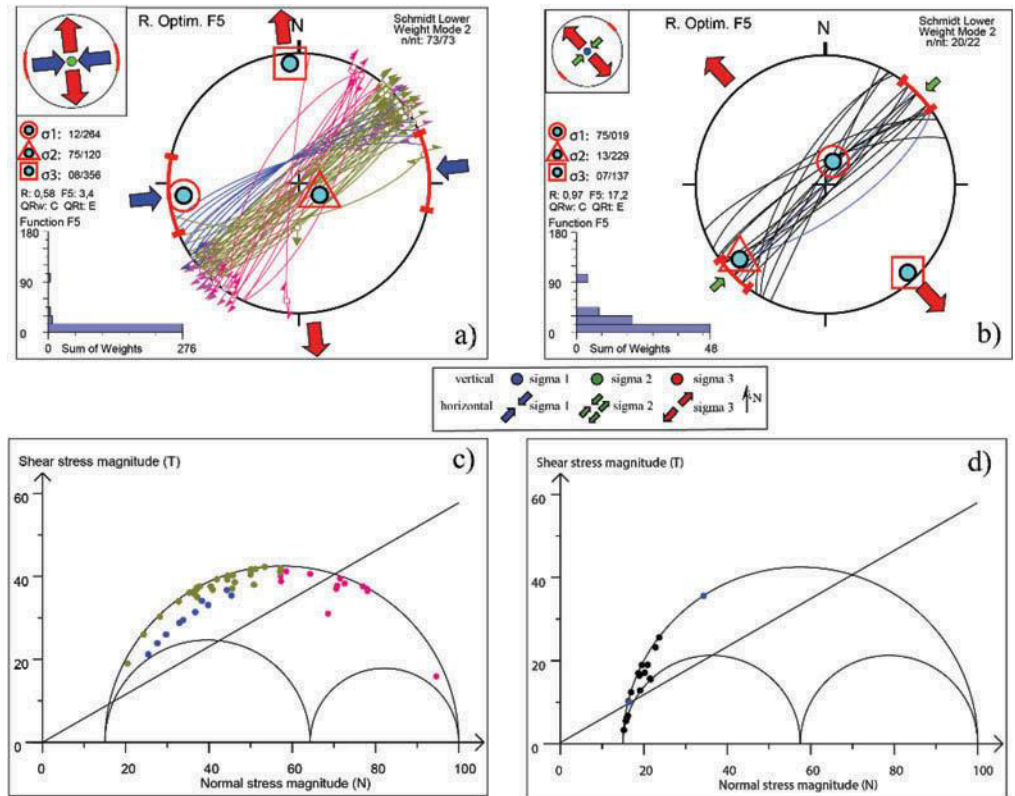


compressive stress. The strike-slip regime, slightly compressional ( $R' = 1,54$ ) has a maximum compressive stress oriented NW-SW ( $319 \pm 21,1/03$ ). The quality rank QRw is medium and the QRT is poor, therefore the solution is not perfectly constrained, but the orientation of the maximum compressive stress fits the range of the solution of  $\tau\sigma_1$  inferred on the field from

Figure 19. Fault slip data and stress inversion results. Lower-hemisphere Schmidt stereo plot of the fault-slip data subsets and corresponding stress tensor. (a) Subset 1 data (Z1) results. (b) Subset 3 (joints) data results. (c) Mohr diagram of subset 1 data. (d) Mohr diagram plots of subset 3 data.



**Figure 20. Fault slip data and stress inversion results. Lower-hemisphere Schmidt stereo plot of the fault-slip data subsets and corresponding stress tensor. (a) Subset 2 data (Z2) results. (b) Subset 4 (joints) data results. (c) Subset 2 data plot in Mohr diagram. (d) Subset 4 data in Mohr diagram.**



extension fractures or horsetails fractures. The Mohr diagram show that some NW-SE to N-S faults have experienced an intense shear stress while others NNE-SSW faults have experienced an intense normal stress relative to the shear stress.

- Stress stage 2 (Figure 20): This last stage is defined by 95 fractures (73 faults and 22 joints), with 29 striated planes of faults. It started with an extension regime (Figure 20b) to slightly strike-slip ( $R' = 1,42$ ) with a principal direction of extension oriented NW-SW of average orientation. Then, it evolved into a strike-slip regime to slightly compressional with a principal stress oriented W-E ( $264 \pm 22,3/12$ ) (Figure 20a). The Mohr diagram of both faults and joints confirms that evolution, of strike slip from joint.

## 6. Discussion

Our field observations show detail strike-slip faults and joints structures that prove that the Inkisi Formation underwent a strike-slip regime. Strike-slip faults show a large range of minor structures across their traces and their profiles, which go from horsetail fractures, extensional fractures in faults linking zones, dilation jogs, wing cracks, en-echelon fractures at their tips and flowers structures (Figure 21).

Rose diagrams and stereograms reveal that faults and joints are organized into two systems of fractures: the first one shows NW-SE to NNE-SSW trends and comprises sinistral faults and joints, the second one shows NE-SW trends and comprises dextral faults and joints too.

Observations indicate a close link between development of joints and strike-slip faults. The presence of plume structures with many arrest lines and calcite veins within their planes suggests that pore fluid pressure probably plays a role in the formation of these fractures (Bons, Elburg, & Gomez-Rivas, 2012; Secor, 1965; Tullis and Tullis J., 1986). Additionally, joints have parallel orientation with faults. On the other hand, some plume joints have overprinted slickensides on their surfaces. Moreover, faults show crystal fiber lineation (striation) and also accretion steps of calcite.



Figure 21. Schematic diagram which idealizes architecture of structures in Inkisi Formation. J1: joints parallel to Z1; J2: joints parallel to Z2; FS: Flower structures; Hr: horsetail splays; e-f: en-echelon fracture.

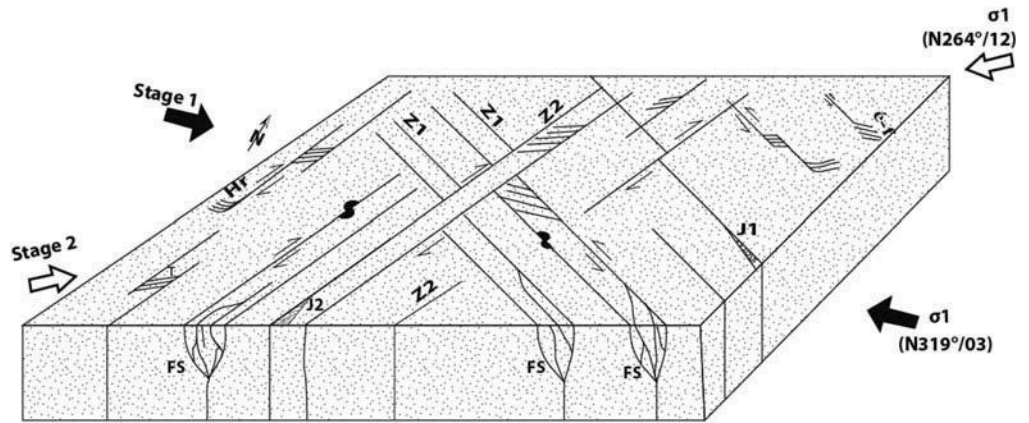


Figure 22. Paleotectonic map of the Permo-triassic transition in African part of Gondwana. The reduce tensor find in Brazzaville are in the same range of orientation as that find in the TRM. Modified by from Delvaux (2001b).

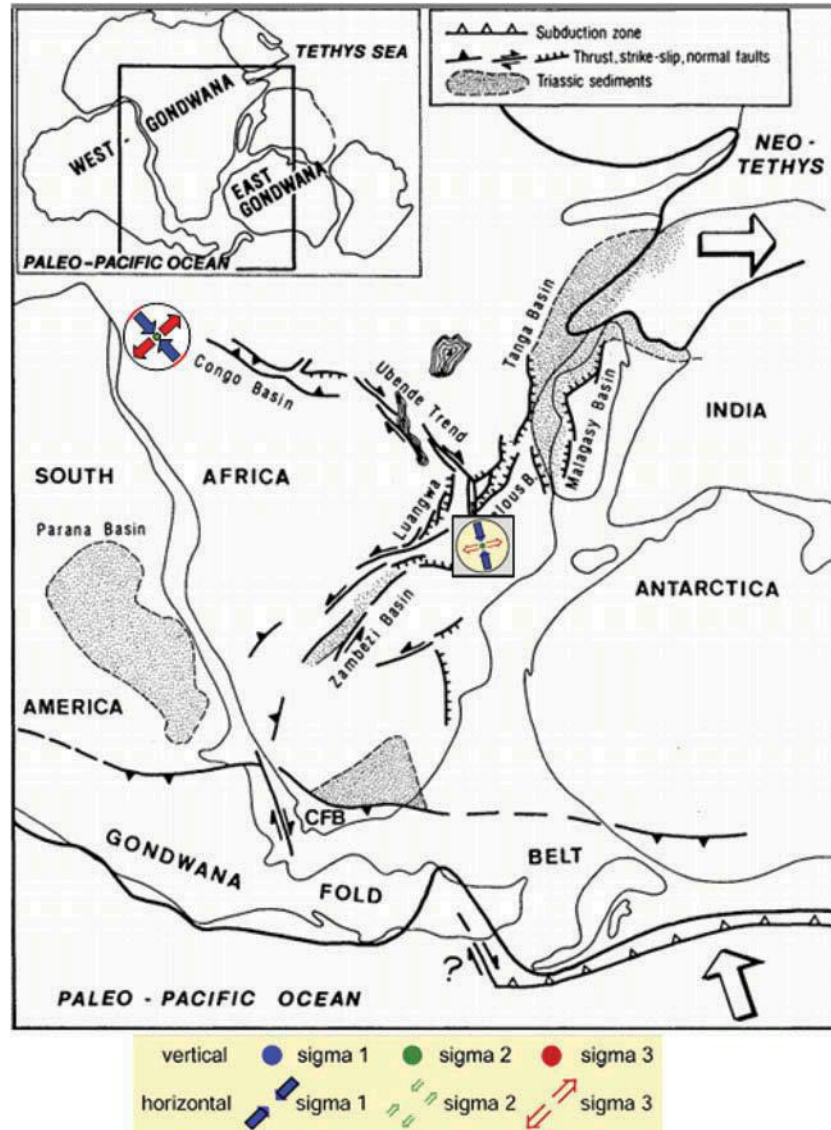
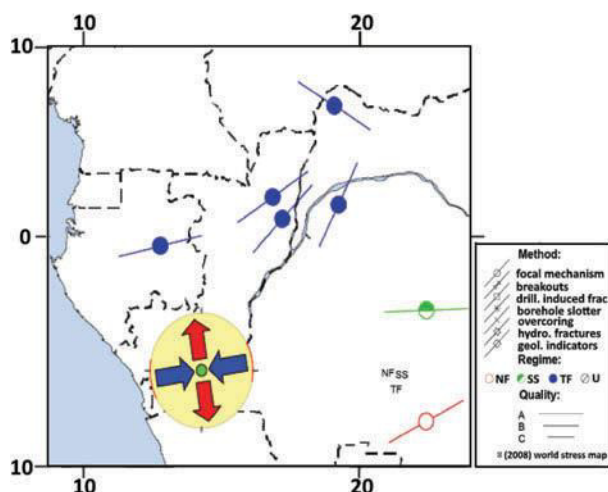


Figure 23. World stress map (2008) and second stress stage reported in the study zone. (Map from [www.world-stress-map.org](http://www.world-stress-map.org)).



This clearly indicates that strike-slip faults nucleated from joints. The same findings have been made by Segall and Pollard (1983), Kim et al. (2004), and Barton (1983). Thus, the two stress stages found from stress inversions method support this field evidence. Both stages of tectonic strike-slip grew from pre-existing joints and some strike-slip faults form small faults with little displacement and others evolved into fault zones and compound fault zones as described in Martel (1990).

Strike-slip faults show clear examples of damage zones structures through their traces as described by Kim et al. (2004) in the classification of fault damage zones. The assumed compressive principal stress on field from horsetail fractures, en-echelon fractures, and extension fractures of N320° supports our determined maximum principal compressive paleostress.

The early stress stage is broadly constrained, because few conjugates faults planes of that stage have been observed on the field. However, these results place a range of limits for the reduced tensor solution with a maximum compressive stress of  $319^{\circ} \pm 21, 1/03$ . Although uncertainties are quite large ( $\pm 21, 1^{\circ}$ ), the orientation of the maximum compressive stress obtained on the field from extension fractures gives an orientation that fits in the interval determine from Win-Tensor. This stress stage has a potential correlation with stresses that propagate from the southern subduction margin of Gondwana at the Permo-Trias which formed the Cap Fold Belt, currently preserved in South Africa. This affirmation is supported by two principal arguments. The first point is that the Inkisi Formation is overlain by Karoo deposits in Angola (Tack et al., 2001), and the Karoo deposits have been deformed in most part of Africa by the subduction that affected the southern margin of Gondwana at Permo-Trias (Catuneanu et al., 2005). Therefore, the Inkisi Formation might have been affected by this tectonic event. More importantly, the reconstruction of paleostress by Delvaux et al. (2012), in the Tanganyika-Rukwa-Malawi (TRM) rift segment in western Tanzania, located the Karoo deposits, gives three stress stages. The second stage which is well constrained, obtained from Karoo deposits of Permian age, called Namwele-Mkolomo coal field, has caused a dextral strike-slip tectonic associated with a transpression that has a subparallel orientation with our first stage (Figure 22). Nonetheless, the stress obtained in TRM is oriented NNW-SSE and cause dextral kinematic, while our orientation is NW-SE and causes sinistral kinematic. This change in kinematic sense might probably be due to a rotation of stress counterclockwise during the collision, as the stress propagated over 2,000 km in the crust (Daly et al., 1992, 1991). The second point is that in Democratic Republic of Congo, in the Congo basin stratigraphic unit, the Banalia Group are correlated to Inkisi Formation (Delpomdor & Pr eat, 2015; Kadima et al., 2011) and they underlay the Karoo deposits that are also affected by the subduction in the southern margin of Gondwana at Permo-Trias (Daly et al., 1992). Therefore, the underlying units of Karoo deposits in the Congo basin must be deformed also. Thus, it proves that the Inkisi Group has been affected by the subduction at Permo-Trias at the southern margin of Gondwana.

The latest stress stage with a sub-horizontal principal compressive stress ( $264^\circ \pm 22,3/12$ ) is not as the early stage well constrained for same reasons, but the maximum compressive stress recorded in extension fractures fits in the same range of that calculated. This stress stage might probably result from ridge push of South Atlantic mid-ocean ridge in continental part. The world map of stress data supports this evidence with the presence of a horizontal compressive stress parallel in orientation with what we determine (Figure 23). This explanation has also been given for Northern Europe and Scandinavia, where the horizontal compressive stress is oriented NW–SE

(Fossen, 2010). This result suggests that the latest stress stage is still active but must be studied through different methods to confirm its activity.

## 7. Conclusion

This paper shows and proves that the Inkisi Formation has been affected by at least two strike-slip tectonic events associated both with a compression, initiated from joints. The early event produces parallel sinistral strike-slip faults and joints and the latter event produces parallel dextral strike-slip faults and joints. Both tectonic events show similar features within their structures (horstail splays, extension fractures, dilation jogs, en-echelon fractures, and flower structures), which form the basis of their identification according to Kim et al. (2004) classification of fault damage zones.

The early tectonic deformation with a horizontal principal compressive stress of  $319^\circ \pm 21,1/03$  (NW–SE) probably results from the subduction at Gondwana southern margin in Permo-Trias. However, the latest tectonic event with a sub-horizontal principal compressive stress ( $264^\circ \pm 22,3/12$ ) (W–E) is potentially generated by ridge push of South Atlantic mid-ocean ridge.

## Acknowledgements

We would like specially to thank Joachim Miyouna for English corrections of the manuscript. Instructive comments of anonymous reviewers substantially improve the quality of the manuscript and were greatly appreciated. We are also grateful to Pr. El Hadji Sow from Cheikh Anta Diop University of Dakar for his advices and encouragements.

## Funding

The author received no direct funding for this research.

## Author details

Timothée Miyouna<sup>1</sup>  
E-mail: [mjyounatim@yahoo.fr](mailto:mjyounatim@yahoo.fr)  
Hardy Medry Dieu-Veill Nkodia<sup>1</sup>  
E-mail: [nkodiahardy@gmail.com](mailto:nkodiahardy@gmail.com)  
Olivier Florent Essouli<sup>1</sup>  
E-mail: [Oflorentessouli@gmail.com](mailto:Oflorentessouli@gmail.com)  
Moussa Dabo<sup>2</sup>  
E-mail: [moussadabo@hotmail.com](mailto:moussadabo@hotmail.com)  
Florent Boudzoumou<sup>1,3</sup>  
E-mail: [boudzoumouflorent@yahoo.fr](mailto:boudzoumouflorent@yahoo.fr)  
Damien Delvaux<sup>4</sup>  
E-mail: [damien.delvaux@africamuseum.be](mailto:damien.delvaux@africamuseum.be)

<sup>1</sup> Marien NGOUABI University, Brazzaville, Republic of Congo.

<sup>2</sup> Cheikh Anta DIOP University, Dakar, Republic of Senegal.

<sup>3</sup> Geosciences Department, National Research Institute in Exact and Natural Sciences (IRSEN) of Brazzaville, Brazzaville, Republic of Congo.

<sup>4</sup> Africa Museum, Leuvensesteenweg 13, Tervuren, B-3080, Belgique.

## Description

This study of deformations in the Inkisi sandstone Formation shows that it is affected by two major directions of NW–SE and WSW–ENE strike-slip faults. The NW–SE faults have displayed sinistral movement, whereas the WSW–ENE faults that offset the previous one have

dextral movement. NW–SE fractures may result from the subduction of Gondwana south margin in the Permo-Trias. The second results from the interplate stress propagation due to the opening of the southern Atlantic ocean.

## Citation information

Cite this article as: Strike-slip deformation in the Inkisi Formation, Brazzaville, Republic of Congo, Timothée Miyouna, Hardy Medry Dieu-Veill Nkodia, Olivier Florent Essouli, Moussa Dabo, Florent Boudzoumou & Damien Delvaux, *Cogent Geoscience* (2018), 4: 1542762.

## References

- Affaton, P, Kalsbeek, F, Boudzoumou, F, Trompette, R, Thrane, K, & Frei, R. (2016). The Pan-African West Congo belt in the Republic of Congo (Congo Brazzaville): Stratigraphy of the Mayombe and West Congo Supergroups studied by detrital zircon geochronology. *Precambrian Research*, 272, 185-202.
- Alkmim, F.F, Marshak, S, Pedrosa-Soares, A.C, Peres, G.G, Cruz, S, & Whittington, A. (2006). Kinematic evolution of the Araçuaí–West Congo orogen in Brazil and Africa: nutcracker tectonics during the Neoproterozoic assembly of Gondwana. *Precambrian Research*, 149, 43–64.
- Alvarez, P., Maurin, J.-C., & Vicat, J.-P. (1995). La formation de l'Inkisi (Supergroupe Ouest-Congolien) en Afrique Centrale (Congo et Bas-Zaïre): Un delta d'âge Paléozoïque comblant un bassin en extension. *Journal of African Earth Sciences*, 20(2), 119–131. doi:10.1016/0899-5362(95)00038-U
- Angelier, J. (1989). From orientation to magnitudes in paleostress determinations using fault slip data. *Journal of Structural Geology*, 11(1/2), 37–50. doi:10.1016/0191-8141(89)90034-5
- Angelier, J. (1994). Fault slip data an paleostress reconstruction. In I. P. Hancock (Ed.), *Continental deformation* (pp. 53–100). Oxford: Pergamon Press.



- Barton, C. C. (1983). Systematic jointing in the Cardium Sandstone along the Bow River, PhD thesis, Alberta, Canada: New Haven, Connecticut, Yale University, 301p.
- Bons, D. P., Elburg, A. M., & Gomez-Rivas, E. (2012). A review of the formation of tectonic veins and their microstructures. *Journal of Structural Geology*, 43, 33–62. doi:10.1016/j.jsg.2012.07.005
- Boudzoumou, F. (1986). La chaîne Ouest-Congolienne et son avant-pays au Congo : relations avec le Mayombien ; sédimentation des séquences d'âge Protérozoïque supérieur. Thèse de doctorat, Université Aix-Marseille, France. 220p.
- Catuneanu, O. (2004). Retroarc foreland systems evolution through time. *Journal of African Earth Sciences*, 38, 225–242. doi:10.1016/j.jafrearsci.2004.01.004
- Catuneanu, O., Wopfener, H., Eriksson, P. G., Cairncross, B., Rubidge, B. S., Smith, R. M., & Hancox, P. J. (2005). The Karoo basins of South-central Africa. *Journal of Earth Sciences*, 43, 211–253.
- Christie-Blick, N., & Biddle, T. K. (1985). Deformation and basin formation along strike-slip faults. *Special Publication Society of Paleontologists and Mineralogists*, N°37, 1–34.
- Cornet, P., & Pourret, G. (1982). Contrôle structural du Congo dans les formations de l'Inkisi en aval de Brazzaville. *Annales Université Brazzaville, 1976-1997* (12–13), 17–28.
- Dadet, P. (1969). Notice explicative de la carte géologique de la République du Congo au 1:500 000 (pp. 103). Orléans: Mémoire BRGM, n°70.
- Daly, M. C., Lawrence, R. S., Dirmu-Tshiband, K., & Matouana, B. (1992). Tectonic evolution of the Cuvette Centrale, Zaïre. *Journal of Geological Society, London*, 149, 539–546. doi:10.1144/gsjgs.149.4.0539
- Daly, M. C., Lawrence, S. R., Kimun'a, D., & Binga, M. (1991). Late Paleozoic deformation in central Africa; a result of distant collision? *Journal Southern American Earth Sciences*, 6, 33–47.
- Davis, G. H., Reynolds, S. J., & Kluth, C. F. (2011). *Structural geology of rocks and regions*. John Wiley & Sons.
- Delpomdor, F., & Prétat, A. (2015). Overview of the Neoproterozoic sedimentary series exposed along margins of the Congo Basin. In M. J. de Wit, F. Guillocheau, & M. C. J. de Wit (eds.), *Geology and resource potential of the Congo basin* (p. 41–58). Berlin, Heidelberg: Springer Berlin Heidelberg.
- Delvaux, D. (1993). The TENSOR program for paleostress reconstruction: Examples from the east African and the Baikal rift zones (Vol. 5, pp. 216). France: Abstract supplement N°1 to Terra Nova.
- Delvaux, D. (2001a). Tectonic an paleostress evolution of the Tanganyika-Rukwa-Malawi rift segment, East African Rift System. In D. P. A. Ziegler, W. Cavazza, A. H. Roberston, & Crasquin-Soleau (Eds.), *Peri-Tethys Memoir 6: Peri Tethyan Rift/Wrench Basins and Passive Margins* (pp. 545–567). Paris 186: Mém. Mus. National Hist. Nat.
- Delvaux, D. (2001b). Karoo rifting in western Tanzania: Precursor of Gondwana breakup. In *Contributions to Geology and Paleontology of Gondwana* (pp. 111–125). Cologne: In honour of Prof. Dr. Helmut Wopfner.
- Delvaux, D., & Sperner, B. (2003). Stress tensor inversion from fault kinematic indicators and focal mechanism data: The TENSOR program. In D. Nieuwland (Ed.), *New Insights into Structural Interpretation and Modelling* (Vol. 212, pp. 75–100). Geological Society, London, Special Publications.
- Delvaux, D., Kervyn, K., Macheyek, S. A., & Temu, E. B. (2012). Geodynamic significance of the TRM segment in the East African Rift (W-Tanzania): Active tectonics and paleostress in the Ufipa plateau and Rukwa basin. *Journal of Structural Geology*, 37, 161–180. doi:10.1016/j.jsg.2012.01.008
- Dianzenza-Ndefi, H. (1983). *Les sédiments du Protérozoïque supérieur et leurs firmations au Nord-Ouest de la Cuvette Congolaise (Afrique Centrale)* (Apport des datations par les méthodes Rb-Sr et K-Ar. Louis Pasteur). Strasbourg, France.
- Fossen, H. (2010). *Structural Geology* (pp. 163). New York: Cambridge University Press.
- Frimel, H. E., Tack, L., Basei, M. S., Nutman, A. P., & Boven, A. (2006). Provenance and chemostratigraphy of the Neoproterozoic West congolian Group in the Democratic Republic of Congo. *Journal of African Earth Sciences*, 46(2006), 221–239. doi:10.1016/j.jafrearsci.2006.04.010
- Hancock, P. L. (1985). Brittle microtectonics: Principles and practice. *Journal of Structural Geology*, 7, 437–457. doi:10.1016/0191-8141(85)90048-3
- Kadima, E., Delvaux, D., Sebagenzi, S.N, Tack, L., & Kabeya, S.M. (2011). Structure and geological history of the Congo Basin: an integrated interpretation of gravity, magnetic and reflection seismic data. *Basin Research*, 23, 499–527.
- Kim, Y.-S., Andrews, J.R, & Sanderson, D.J. (2000). Damage zones around strike-slip fault systems and strike-slip fault evolution, Crackington, Haven, southwest England. *Geoscience Journal*, 4, 53–72.
- Kim, Y.-S. P., Peacock, D. C., & Sanderson, J. (2004). Fault damage zones. *Journal of Structural Geology*, 26, 503–517. doi:10.1016/j.jsg.2003.08.002
- Martel, S. J. (1990). Formation of compound strike-slip zones, Mount Abbot quadrangle, California. *Journal of Structural Geology*, 12(7), 869–882. doi:10.1016/0191-8141(90)90060-C
- Mickala, O. R., Vidal, L., Boudzoumou, F., Affaton, F., Vandamme, D., Borshneck, D., ... Miche, H. (2014). Geochemical characterization of the Marinoan “Cap Carbonate” of the Niari-Nyanga Basin (Central Africa). *Precambrian research*, 255, Part 1, 357–380.
- Oesterlen, M. (1976). Karoo-System und präkambrische Unterlage im nördlichen Angola-I. Stratigraphie, Tektonik und Petrographie. *Geologisches Jahrbuch, Reihe B*, 20, 3–55, Hannover.
- Oesterlen, M. (1979). Karoo system und präkambrische unterlage im nördlichen Angola-II. Diagenese un Sedimentologie des Karoo Systems. *Geologisches Jahrbuch, Reihe B*, 36, 3–41, Hannover.
- Olson, E. J., & Pollard, D. D. (1991). The initiation and growth of en échelon veins. *Journal of Structural Geology*, 13(5), 595–608. doi:10.1016/0191-8141(91)90046-L
- Poidevin, J. L. (2007). Stratigraphie isotopique du strontium et datation des formations carbonatées et glaciogéniques néoproterozoïques du Nord et de l'Ouest du craton du Congo. *Comptes Rendus Geoscience*, 339, 259–273. doi:10.1016/j.crte.2007.02.007
- Pollard, D., & Aydin, A. (1988). Progress in understanding jointing over the past century. *The Geological Society of America*, 100, 1181–1204. doi:10.1130/0016-7606(1988)100<1181:PIUJOT>2.3.CO;2
- Secor, D. J. (1965). Role of fluid pressure in jointing. *American Journal of Science*, 263, 633–646. doi:10.2475/ajs.263.8.633
- Segall, P., & Pollard, D. D. (1983). Nucleation and growth strike-slip faults in granite. *Journal of Geophysical Research*, 14, 555–568. doi:10.1029/JB088iB01p00555
- Straathof, G. B. (2011). *Neoproterozoic low latitude glaciations: An African perspective*. PhD, thesis, University of Edinburgh, U.K, Edinburgh, p. 263

- Sylvester, A. G. (1988). Strike slip faults. *Geological Society of America Bulletin*, 100, 1666–1703. doi:10.1130/0016-7606(1988)100<1666:SSF>2.3.CO;2
- Tack, L., Delvaux, D., Kadima, E., Delpomdor, F., Tahon, A., Dumont, P., ... Dewaele, S. (2008). The 1.000 m thick Redbeds sequence of the Congo River Basin (CRB): A generally overlooked testimony in Central Africa of post-Gondwana amalgamation (550 Ma) and pre-Karoo break-up (320 Ma). *22nd Colloquium of African Geology, Hammamet, Tunisia, November 4-6, 2008, Abstract book*, 86-88.
- Tack, L., Wingate, M., Liégeois, J.-P., Fernandez-Alonso, M., & Deblond, A. (2001). Early Neoproterozoic magmatism (1000-910 MA) of the Zadinian and Mayumbian Groups (Bas-Congo): Onset of Rodinian rifting at western edge of the Congo craton. *Precambrian Research*, 110, 277–306. doi:10.1016/S0301-9268(01)00192-9
- Tait, J., Delpomdor, F., Pr at, A., Tack, L., Straathof, G., & Nkula, V. K. (2011). Neoproterozoic sequences of the West Congo and Lindi/Ubangi Supergroups in the Congo Craton, Central Africa. *Geological Society, London, Memoirs*, 36, 185–194.
- Tullis, T. E., & Tullis, J. (1986). Experimental rock deformation techniques, In Hobbs B. E., & Heard H. C. (eds.), *Mineral and rock deformation; laboratory studies; the Paterson volume: Geophysical Monograph*, Monash University, Clayton, Victoria, Australia, v. 36, p. 297–324.

## Appendices

**Table A1. Input data table of joints and faults slip in Win-Tensor with primary subset associated. Type (1: fault with slip line; 3: faults with tension fracture, 4: plane of fracture); column slip sense (S: Sinistral; D: dextral; T: tension); column confidence level (C: certain; P: probable)**

Id	Properties			Fracture plane		Slip line/tension fracture		Slip	Conf.	Weight	Activ.	Striae	Subset
	Format	Type		Dip	Dip-Direction	Plunge/Dip	Azimuth/Dip-Dir.						
Bro-1	11	4		80	80			S	C	2,0	1		1,0
Bro-2	11	4		80	116			D	C	2,0	1		2,0
Bro-3	11	4		80	268			T	C	2,0			3,0
Bro-4	11	4		85	325			D	C	2,0	1		2,0
Bro-5	11	4		90	180			D	C	2,0	1		4,0
Bro-6	11	4		70	263			S	C	2,0	1		1,0
Bro-7	11	4		75	328			D	C	2,0	1		2,0
Bro-8	11	4		75	325			D	C	2,0	1		2,0
Bro-9	11	1		80	320	4	49	D	C	2,0	1	2	2,0
Bro-10	11	4		85	135			D	C	2,0	1		2,0
Bro-11	11	4		85	245			S	C	2,0	1		1,0
Bro-12	11	1		79	315	3	44	D	C	2,0	1	2	2,0
Bro-13	11	4		75	300			T	P	2,0			4,0
Bro-14	11	4		80	146			D	C	2,0	1		2,0
Bro-15	11	1		85	152	1	62	D	C	2,0	1	2	2,0
Bro-16	11	3		90	72	90	195		P	2,0	1	2	1,0
Bro-17	11	1		70	146	1	56	D	C	2,0	1	2	2,0
Bro-18	11	4		80	235			T	P	2,0			4,0
Bro-19	11	4		85	267			S	C	2,0	1		1,0

(Continued)



**Table A1. (Continued)**

Id	Properties			Fracture plane		Slip line/tension fracture		Slip	Conf.	Weight	Activ.	Striae	Subset
	Format	Type	Dip	Dip-Direction	Plunge/Dip	Azimuth/Dip-Dir.	Sense						
Bro-20	11	3	90	72	90	194			P	2,0	1	2	1,0
Bro-21	11	4	80	235			S		P	2,0	1		4,0
Bro-22	11	3	85	267	75	58			P	2,0	1	2	1,0
Bro-23	11	3	85	267	75	52			P	2,0	1	2	1,0
Bro-24	11	1	75	133	2	43	D		C	2,0	1	2	2,0
Bro-25	11	4	85	318			D		C	2,0	1		2,0
Bro-26	11	3	85	267	75	52			P	2,0	1	2	1,0
Bro-27	11	4	75	65			S		C	2,0	1		1,0
Bro-28	11	4	90	135			D		C	2,0	1		2,0
Bro-29	11	4	90	50			T		P	2,0			4,0
Bro-30	11	1	75	145	1	55	D		C	2,0	1	2	2,0
Bro-31	11	3	85	250	65	17			P	2,0	1	2	1,0
Bro-32	11	1	85	115	5	25	D		C	2,0	2	2	2,0
Bro-33	11	3	85	262	85	220			P	2,0	1	2	1,0
Bro-34	11	3	85	262	85	210			P	2,0	1	2	1,0
Bro-35	11	3	85	73	85	195			P	2,0	1	2	1,0
Bro-36	11	4	90	299			D		P	2,0	1		2,0
Bro-37	11	3	85	73	85	210			P	2,0	1	2	1,0
Bro-38	11	3	85	74	85	220			P	2,0	1	2	1,0
Bro-39	11	4	90	252			M		C	2,0	1		1,0
Bro-40	11	4	75	332			D		C	2,0	1		2,0
Bro-41	11	1	85	268	4	178	S		C	2,0	1	2	1,0

(Continued)

**Table A1. (Continued)**

Id	Properties			Fracture plane		Slip line/tension fracture		Slip	Conf.	Weight	Activ.	Striae	Subset
	Format	Type	Dip	Dip-Direction	Plunge/Dip	Azimuth/Dip-Dir.	Sense						
Bro-42	11	1	82	300	1	210	D	C	2,0	1	2	2,0	
Bro-43	11	4	90	129			D	C	2,0	1		2,0	
Bro-44	11	4	70	273			S	C	2,0	1		1,0	
Bro-45	11	3	85	261	87	227		P	2,0	1	2	1,0	
Bro-46	11	4	75	343			D	C	2,0	1		2,0	
Bro-47	11	4	85	244			S	C	2,0	1		1,0	
Bro-48	11	1	70	245	4	157	S	C	2,0	1	2	1,0	
Bro-49	11	1	65	300	4	212	D	C	2,0	1	2	2,0	
Bro-50	11	1	80	248	1	158	S	C	2,0	1	2	1,0	
Bro-51	11	3	80	248	75	199		P	2,0	1	2	1,0	
Bro-52	11	4	75	339			T	P	2,0			4,0	
Bro-53	11	4	70	330			T	P	2,0			4,0	
Bro-54	11	4	80	264			S	P	2,0	1		1,0	
Bro-55	11	4	85	156			D	P	2,0	1		2,0	
Bro-56	11	4	75	336			D	P	2,0	1		2,0	
Bro-57	11	1	75	266	5	177	S	C	2,0	1	2	1,0	
Bro-58	11	3	75	266	85	220		P	2,0	1	2	1,0	
Bro-59	11	3	75	266	86	220		P	2,0	1	2	1,0	
Bro-60	11	4	80	135			D	C	2,0	1		2,0	
Bro-61	11	4	80	144			T	P	2,0			4,0	
Bro-62	11	3	85	261	86	236		P	2,0	1	2	1,0	
Bro-63	11	4	80	325			T	P	2,0			4,0	

(Continued)

**Table A1. (Continued)**

Id	Properties				Fracture plane		Slip line/tension fracture		Slip	Conf.	Weight	Activ.	Striae	Subset
	Format	Type	Dip	Dip-Direction	Plunge/Dip	Azimuth/Dip-Dir.	Sense	Level						
Bro-64	11	4	80	65					T	P	2,0			4,0
Bro-65	11	4	80	326					T	P	2,0			4,0
Bro-66	11	4	60	88					T	P	2,0			4,0
Bro-67	11	4	80	326					T	P	2,0			4,0
Bro-68	11	4	85	246					M	P	2,0	1		1,0
Bro-69	11	4	85	247					S	P	2,0	1		1,0
Bro-70	11	4	80	254					S	P	2,0	1		1,0
Bro-71	11	4	80	245					S	P	2,0	1		1,0
Bro-72	11	4	75	331					D	P	2,0	1		2,0
Bro-73	11	4	80	267					S	P	2,0	1		1,0
Bro-74	11	4	78	68					S	P	2,0	1		1,0
Bro-75	11	4	75	320					D	P	2,0	1		2,0
Bro-76	11	4	80	245					S	P	2,0	1		1,0
Bro-77	11	3	80	245	80	210				P	2,0	1	2	1,0
Bro-78	11	3	85	245	85	213				P	2,0	1	2	1,0
Bro-79	11	1	85	130	5	40			D	C	2,0	1	2	2,0
Bro-80	11	4	90	130					D	C	2,0	1		2,0
Bro-81	11	4	90	78					S	C	2,0	1		1,0
Bro-82	11	3	90	78	90	36				P	2,0	1	2	1,0
Bro-83	11	3	90	78	90	38				P	2,0	1	2	1,0
Bro-84	11	1	90	75	5	345			S	C	2,0	1	2	1,0
Bro-85	11	4	90	135					D	C	2,0	1		2,0

(Continued)

**Table A1. (Continued)**

Id	Properties			Fracture plane		Slip line/tension fracture		Slip	Conf.	Weight	Activ.	Striae	Subset
	Format	Type	Dip	Dip-Direction	Plunge/Dip	Azimuth/Dip-Dir.	Sense						
Bro-86	11	3	88	263	70	210			P	2,0	1	2	1,0
Bro-87	11	4	90	139				D	C	2,0	1		2,0
Bro-88	11	4	89	69				S	C	2,0	1		1,0
Bro-89	11	4	80	72				S	C	2,0	1		1,0
Bro-90	11	4	85	145				D	C	2,0	1		2,0
Bro-91	11	4	85	148				D	C	2,0	1		2,0
Bro-92	11	1	85	148	5	58		D	C	2,0	1	2	2,0
Bro-93	11	4	85	256				S	C	2,0	1		1,0
Bro-94	11	4	85	325				D	C	2,0	1		2,0
Bro-95	11	1	90	245	3	155		S	C	2,0	1	2	1,0
Bro-96	11	3	90	245	87	210			P	2,0	1	2	1,0
Bro-97	11	4	90	252				T	C	2,0			3,0
Bro-98	11	4	85	138				D	C	2,0	1		2,0
Bro-99	11	4	85	145				D	C	2,0	1		2,0
Bro-100	11	4	85	79				S	C	2,0	1		1,0
Bro-101	11	4	90	82				S	C	2,0	1		1,0
Bro-102	11	4	85	135				D	C	2,0	1		2,0
Bro-103	11	4	85	130				D	C	2,0	1		2,0
Bro-104	11	3	85	130	85	190			P	2,0	1	2	2,0
Bro-105	11	3	85	135	85	195			P	2,0	1	2	2,0
Bro-106	11	3	90	88	85	208			P	2,0	1	2	1,0
Bro-107	11	3	90	88	85	142			P	2,0	1	2	1,0

(Continued)



**Table A1. (Continued)**

Id	Properties			Fracture plane		Slip line/tension fracture		Slip	Conf.	Weight	Activ.	Striae	Subset
	Format	Type	Dip	Dip-Direction	Plunge/Dip	Azimuth/Dip-Dir.	Sense						
Bro-108	11	4	79	258			S	C	2,0	1		1,0	
Bro-109	11	4	80	144			D	C	2,0	1		2,0	
Bro-110	11	4	90	322			D	C	2,0	1		2,0	
Bro-111	11	3	80	75	90	222		P	2,0	1	2	1,0	
Bro-112	11	3	80	265	90	230		P	2,0	1	2	1,0	
Bro-113	11	3	65	250	70	220		P	2,0	1	2	1,0	
Bro-114	11	1	90	130	2	40	D	C	2,0	1	2	2,0	
Bro-115	11	4	75	269			S	C	2,0	1		1,0	
Bro-116	11	4	90	299			D	C	2,0	1		2,0	
Bro-117	11	4	70	273			S	C	2,0	1		1,0	
Bro-118	11	4	85	244			S	C	2,0	1		1,0	
Bro-119	11	4	90	75			S	C	2,0	1		1,0	
Bro-120	11	4	75	339			D	C	2,0	1		2,0	
KO-1	11	4	80	104			S	P	2,0	1		1,0	
KO-2	11	4	85	94			S	P	2,0	1		1,0	
KO-3	11	4	80	82			S	P	2,0	1		1,0	
KO-4	11	1	85	89	2	359	S	C	2,0	1	2	1,0	
KO-5	11	4	82	62			T	P	2,0			4,0	
KO-6	11	4	85	201			T	P	2,0			4,0	
KO-7	11	4	85	299			T	P	2,0			4,0	
KO-8	11	4	85	280			T	P	2,0			4,0	
KO-9	11	3	90	89	85	236		P	2,0	1	2	1,0	

(Continued)

**Table A1. (Continued)**

Id	Properties			Fracture plane		Slip line/tension fracture		Slip	Conf.	Weight	Activ.	Striae	Subset
	Format	Type	Dip	Dip-Direction	Plunge/Dip	Azimuth/Dip-Dir.	Sense						
KO-10	11	4	85	275				S	C	2,0	1		1,0
KO-11	11	3	85	62	90	225			P	2,0	1	2	1,0
KO-12	11	4	86	99				S	C	2,0	1		1,0
KO-13	11	3	86	99	80	235			P	2,0	1	2	1,0
KO-14	11	3	90	62	85	16			P	2,0	1	2	1,0
KO-15	11	4	80	102				T	P	2,0			4,0
KO-16	11	4	90	13				T	P	2,0			4,0
KO-17	11	4	70	250				T	P	2,0			4,0
KO-18	11	4	80	62				T	P	2,0			4,0
KO-19	11	4	90	115				T	P	2,0			4,0
KO-20	11	4	80	189				T	P	2,0			4,0
KO-21	11	4	85	274				T	P	2,0			4,0
KO-22	11	4	82	68				T	P	2,0			4,0
KO-23	11	4	82	68				T	P	2,0			4,0
KO-24	11	4	90	68				T	P	2,0			4,0
KO-25	11	4	90	99				T	P	2,0			4,0
KO-26	11	4	75	325				D	P	2,0	1		2,0
KO-27	11	3	80	253	85	23			P	2,0	1	2	1,0
KO-28	11	4	80	242				S	C	2,0	1		1,0
KO-29	11	4	88	245				S	C	2,0	1		1,0
KO-30	11	3	85	250	85	13			P	2,0	1	2	1,0
KO-31	11	3	85	250	85	209			P	2,0	1	2	1,0

(Continued)

**Table A1. (Continued)**

Id	Properties			Fracture plane		Slip line/tension fracture		Slip	Conf.	Weight	Activ.	Striae	Subset
	Format	Type	Dip	Dip-Direction	Plunge/Dip	Azimuth/Dip-Dir.	Sense						
KO-32	11	4	85	175				D	P	2,0	1		4,0
KO-33	11	4	85	300				D	P	2,0	1		2,0
KO-34	11	4	85	300				D	P	2,0	1		2,0
KO-35	11	4	85	222				S	P	2,0	1		4,0
KO-36	11	4	90	125				D	C	2,0	1		2,0
KO-37	11	3	80	280	85	55			P	2,0	1	2	1,0
KO-38	11	4	65	89				S	C	2,0	1		1,0
KO-39	11	4	85	210				D	C	2,0	1		4,0
KO-40	11	4	85	45				T	C	2,0			3,0
KO-41	11	4	85	40				T	C	2,0			3,0
KO-42	11	4	85	252				D	C	2,0	1		1,0
KO-43	11	4	85	310				D	C	2,0	1		2,0
KO-44	11	1	85	130	1	40		D	C	2,0	1	2	2,0
KO-45	11	4	75	20				T	C	2,0			4,0
KO-46	11	1	85	245	2	155		S	C	2,0	1	2	1,0
KO-47	11	1	80	310	5	220		D	C	2,0	1	2	2,0
KO-48	11	1	80	325	2	235		D	C	2,0	1	2	2,0
KO-49	11	1	80	100	2	10		S	C	2,0	1	2	1,0
KO-50	11	3	80	100	80	55			P	2,0	1	2	1,0
KO-51	11	1	70	96	2	6		S	C	2,0	1	2	1,0
KO-52	11	4	90	235				D	C	2,0	1		4,0
KO-53	11	4	85	310				T	C	2,0			4,0

(Continued)

**Table A1. (Continued)**

Id	Properties			Fracture plane		Slip line/tension fracture		Slip	Conf.	Weight	Activ.	Striae	Subset
	Format	Type	Dip	Dip-Direction	Plunge/Dip	Azimuth/Dip-Dir.	Sense						
KO-54	11	4	85	50				D	C	2,0	1		4,0
KO-55	11	4	75	75				T	P	2,0			4,0
KO-56	11	4	80	55				T	P	2,0			4,0
KO-57	11	4	90	135				T	P	2,0			4,0
KO-58	11	4	80	30				T	P	2,0			4,0
KO-59	11	4	85	142				T	P	2,0			4,0
KO-60	11	4	70	302				T	P	2,0			4,0
KO-61	11	4	75	64				T	P	2,0			4,0
KO-62	11	4	85	54				T	P	2,0			4,0
KO-63	11	4	85	20				T	P	2,0			4,0
KO-64	11	4	85	39				T	P	2,0			4,0
KO-65	11	4	90	50				T	P	2,0			4,0
KO-66	11	4	85	130				T	P	2,0			4,0
KO-67	11	4	85	130				T	P	2,0			4,0
KO-68	11	4	85	68				T	C	2,0			3,0
KO-69	11	4	70	145				T	C	2,0			3,0
KO-70	11	4	85	89				T	C	2,0			3,0
KO-71	11	4	65	49				T	C	2,0			4,0
KO-72	11	4	70	142				D	C	2,0	1		2,0
KO-73	11	4	70	62				S	C	2,0	1		1,0
KO-74	11	4	82	42				T	C	2,0			3,0
KO-75	11	4	90	142				T	C	2,0			4,0

(Continued)



**Table A1. (Continued)**

Id	Properties			Fracture plane		Slip line/tension fracture		Slip	Conf.	Weight	Activ.	Striae	Subset
	Format	Type	Dip	Dip-Direction	Plunge/Dip	Azimuth/Dip-Dir.	Sense						
KO-76	11	4	85	135				D	C	2,0	1		2,0
KO-77	11	4	90	313				T	C	2,0			3,0
KO-78	11	4	85	135				T	P	2,0			4,0
KO-79	11	4	85	315				T	P	2,0			4,0
KO-80	11	4	90	75				T	P	2,0			4,0
KO-81	11	4	90	110				T	P	2,0			4,0
KO-82	11	4	85	74				T	P	2,0			4,0
KO-83	11	4	80	33				T	P	2,0			4,0
KO-84	11	4	85	104				S	C	2,0	1		1,0
KO-85	11	3	85	104	90	224			P	2,0	1	2	1,0
KO-86	11	4	90	34				D	P	2,0	1		4,0
KO-87	11	4	75	85				T	P	2,0			4,0
KO-88	11	4	89	241				T	P	2,0			4,0
KO-89	11	1	70	90	2	0		S	C	2,0	2	2	1,0
KO-90	11	4	85	286				S	C	2,0	2		1,0
KO-91	11	4	85	22				D	C	2,0	2		4,0
KO-92	11	4	80	45				D	C	2,0	2		4,0
KO-93	11	4	85	240				S	C	2,0	2		4,0
KO-94	11	3	70	140	60	203			P	2,0	1	2	2,0
KO-95	11	3	90	75	60	30			P	2,0	1	2	1,0
KO-96	11	4	90	322				D	C	2,0	1		2,0
KO-97	11	1	85	135	2	45		D	C	2,0	1	2	2,0

(Continued)

**Table A1. (Continued)**

Id	Properties			Fracture plane		Slip line/tension fracture		Slip	Conf.	Weight	Activ.	Striae	Subset
	Format	Type	Dip	Dip-Direction	Plunge/Dip	Azimuth/Dip-Dir.	Sense						
KO-98	11	4	85	145				D	C	2,0	1		2,0
KO-99	11	4	85	138				D	C	2,0	1		2,0
KO-100	11	1	85	139	3	50		D	C	2,0	1	2	2,0
KO-101	11	4	90	130				D	C	2,0	1		2,0
KO-102	11	4	90	130				D	C	2,0	1		2,0
KO-103	11	4	70	75				D	C	2,0	1		1,0
KO-104	11	3	85	109	90	235			P	2,0	1	2	1,0
KO-105	11	3	80	260	80	205			P	2,0	1	2	1,0
KO-106	11	3	87	87	80	225			P	2,0	1	2	1,0
KO-107	11	3	87	87	80	210			P	2,0	1	2	1,0
KO-108	11	3	85	100	90	239			P	2,0	1	2	1,0
KO-109	11	1	90	100	10	10		S	C	2,0	1	2	1,0
KO-110	11	1	90	100	21	10		S	C	2,0	1	2	1,0
KO-111	11	4	80	60				T	C	2,0			3,0
KO-112	11	1	85	240	20	152		S	C	2,0	2	2	1,0
KO-113	11	1	90	255	15	165		S	C	2,0	2	2	1,0
KO-114	11	4	90	239				T	C	2,0			3,0
KO-115	11	4	90	100				T	C	2,0			3,0
KO-116	11	3	90	105	90	226			P	2,0	1	2	1,0
KO-117	11	3	80	258	90	200			P	2,0	1	2	1,0
KO-118	11	4	80	319				D	C	2,0	1		2,0
KO-119	11	3	90	87	90	229			P	2,0	1	2	1,0

(Continued)

**Table A1. (Continued)**

Id	Properties			Fracture plane		Slip line/tension fracture		Slip	Conf.	Weight	Activ.	Striae	Subset
	Format	Type	Dip	Dip-Direction	Plunge/Dip	Azimuth/Dip-Dir.	Sense						
KO-120	11	1	90	254	6	164	S	C	2,0	1	2	1,0	
KO-121	11	1	90	135	5	45	D	C	2,0	1	2	2,0	
KO-122	11	1	90	145	5	55	D	C	2,0	1	2	2,0	
KO-123	11	3	90	254	90	210		P	2,0	1	2	1,0	
KO-124	11	3	90	264	90	209		P	2,0	1	2	1,0	
KO-125	11	1	80	259	5	169	S	C	2,0	1	2	1,0	
KO-126	11	1	80	269	3	180	S	C	2,0	1	2	1,0	
KO-127	11	4	80	268			T	C	2,0			3,0	
KO-128	11	4	90	258			T	C	2,0			3,0	
KO-129	11	1	70	115	2	25	D	C	2,0	2	2	2,0	
KO-130	11	3	85	322	90	185		P	2,0	1	2	2,0	
KO-131	11	1	85	120	5		D	C	2,0	1	2	2,0	
KO-132	11	1	70	135	2		D	C	2,0	1	2	2,0	
KO-133	11	1	90	142	3	32	D	C	2,0	1	2	2,0	
KO-134	11	1	68	166	2	45	D	C	2,0	1	2	2,0	
KO-135	11	1	85	275	10	77	D	C	2,0	1	2	2,0	





© 2018 The Author(s). This open access article is distributed under a Creative Commons Attribution (CC-BY) 4.0 license.

You are free to:

Share — copy and redistribute the material in any medium or format.

Adapt — remix, transform, and build upon the material for any purpose, even commercially.

The licensor cannot revoke these freedoms as long as you follow the license terms.

Under the following terms:

Attribution — You must give appropriate credit, provide a link to the license, and indicate if changes were made.

You may do so in any reasonable manner, but not in any way that suggests the licensor endorses you or your use.

No additional restrictions

You may not apply legal terms or technological measures that legally restrict others from doing anything the license permits.



**Cogent Geoscience (ISSN: 2331-2041) is published by Cogent OA, part of Taylor & Francis Group.**

**Publishing with Cogent OA ensures:**

- Immediate, universal access to your article on publication
- High visibility and discoverability via the Cogent OA website as well as Taylor & Francis Online
- Download and citation statistics for your article
- Rapid online publication
- Input from, and dialog with, expert editors and editorial boards
- Retention of full copyright of your article
- Guaranteed legacy preservation of your article
- Discounts and waivers for authors in developing regions

**Submit your manuscript to a Cogent OA journal at [www.CogentOA.com](http://www.CogentOA.com)**

